Quasi-three-dimensional numerical model for flow through flexible, rigid, submerged and non-submerged vegetation

K. S. Erduran and V. Kutija

ABSTRACT

The effects of the resistance caused by vegetation on flow velocity and water depth has become a major interest for ecologists and those who deal with river restoration projects. Some numerical and experimental works have been performed to analyse and formulate the drag effects induced by vegetation. Here we introduce a quasi-three-dimensional (Q3D) numerical solution, which is constructed by coupling the finite volume solution of the two-dimensional shallow water equations with a finite difference solution of Navier–Stokes equations for vertical velocity distribution. The drag forces are included in both sets of equations. Turbulence shear stresses are computed in two alternative ways: the parabolic eddy viscosity approach with a correction term introduced in this study, and a combination of the eddy viscosity and mixing length theories in the vertical direction. In order to deal with flexible vegetation, a cantilever beam theory is used to compute the deflection of the vegetation. The model COMSIM (complex flow simulations) has been developed and applied in experimental cases. The results are shown to be satisfactory.

Key words | flexible and rigid vegetation, quasi-three-dimensional model, submerged and non-submerged vegetation

K. S. Erduran (corresponding author)
V. Kutija
WRSRL,
Department of Civil Engineering,
University of Newcastle,
Newcastle upon Tyne NE1 7RU,
UK
Tel.: +44 191 2225842;
Fax: +44 191 2226669;
E-mail: *Kutsi.Erduran@ncl.ac.uk, Vedrana.Kutija@ncl.ac.uk*

INTRODUCTION

Understanding the behaviour of flow through vegetation is of interest to designers dealing with wetland, floodplain and river lining projects. Vegetation influences the flow resistance, which is a major factor determining water level and velocity distribution (Wu *et al.* 1999). The main impact of vegetation on flow is that it causes a drag, resulting in momentum losses (Fischenich 2000). Consequently, vegetation causes sedimentation (Li & Shen 1973).

Many attempts have been made to find an accurate representation of the behaviour of flow through vegetation. This is not a trivial task and most of the previous work is based on experiments (Li & Shen 1973; Temple 1986; Fathi-Maghadam & Kouwen 1997; Wu *et al.* 1999) and yet it is not clear how to estimate the flow resistance (Fathi-Maghadam & Kouwen 1997; Darby, 1999). This may be because there are so many factors that influence the resistance. Stiffness, diameter, height, distribution, density and type of vegetation and height of flow are examples of these factors (Li & Shen 1973; Chow 1973; Wu *et al.* 1999). Apart from these, there are some other conditions that influence the resistance and consequently the flow components, such as whether vegetation is submerged or not (Fischenich 2000) and whether vegetation is flexible or rigid (Kutija & Hong 1996). Moreover, Wu *et al.* (2001) show that large vegetation, such as trees, causes not only a drag effect but also a blockage effect.

The simplest approach to compute flow through vegetation would be to use Manning's formula together with the most suitable constant Manning's value specifically given for vegetated surface with different vegetation types and arrangements by Chow (1973). One of the earliest and commonly used methods to estimate Manning's n for flow through vegetation is known as the n-VR method. The method was developed by the US

Department of Agriculture (USDA 1947). Alternatively, Kouwen (1992) proposes a method for the evaluation of vegetative flow resistance. This approach is known as the *MEI* (or relative roughness) method. The most important feature of the method is that it takes account of bending of vegetation. Petryk & Bosmajian III (1975) introduce a method, which is based on conservation of momentum for one-dimensional steady uniform flow, including drag forces.

Among the numerical approaches previously developed, a model introduced by Kutija & Hong (1996) covers a variety of cases, namely computation of flow through submerged, non-submerged, flexible and rigid vegetation. The model is based on the one-dimensional horizontal momentum equation solved in the vertical direction. One of the most innovative features of the model is that bending of the vegetation and the deflection caused by a water load is computed using cantilever beam theory (Timoshenko 1955). Saowapon & Kouwen (1989) also use this theory for the same purpose. Darby (1999) describes a one-dimensional (1D) model, Hmodel2, based on the momentum and continuity equations. The model is constructed to be suitable for computation of flow through vegetation under conditions of flexible and rigid vegetation. This model uses Kouwen's (1992) approach in order to compute flow resistance for the flexible vegetation and is suitable for steady uniform flow conditions. Simoes & Wang (1997) introduce a Q3D model. They achieve turbulence closure by means of an eddy viscosity approach and they assume a parabolic eddy viscosity distribution with an additional viscosity due to drag effects. Their 3D model is suitable for simulation of flow through rigid vegetation. Shimizu & Tsujimoto (1997) also apply a turbulence model, applicable only for rigid vegetation. Recently, Fischer-Antze *et al.* (2001) introduce a 3D $k-\varepsilon$ turbulence model, which is suitable for rigid non-submerged vegetation.

The above methods show a varying level of complexity, from simple Manning's formula to the more advanced 3D $k-\varepsilon$ turbulence model, and have at least one drawback. Manning's formula is suitable for steady uniform flow and the choice of Manning's n is not well defined. The applicability of the *n-VR* method is restricted and is found to be not suitable for a bed slope less than 1–2% (Kouwen & Li 1980). The *MEI* method requires several empirical coefficients to be known before computation and it is only one-dimensional. The remaining methods are also either one-dimensional (not capable of capturing realistic flow behaviour) or they are suitable only for rigid vegetation. In nature a great deal of vegetation falls under herbaceous species and they are flexible. To the authors' knowledge there is no 3D numerical model which is applicable for flow through flexible vegetation.

Here we introduce a Q3D numerical method for the simulation of flow through flexible, rigid, submerged and non-submerged vegetation.

The adopted approach is mechanistic and not empirical, as in most of the other work in the field. Hence, cantilever beam theory (Timoshenko 1955) is used for estimation of the deflection of the vegetation. The transition between rigid and flexible vegetation is smooth as the same algorithms are used and behaviour depends on the stiffness of the plants (stiffness of a material is its resistance to deflection and is also known as the modulus of elasticity) and the flow conditions.

In order to provide alternative solutions to turbulence closure, the turbulent shear stresses are computed in two different ways: the parabolic eddy viscosity approach with a correction term introduced here, and the combination of the eddy viscosity and the mixing length theories. Slip and non-slip boundary conditions at the channel bottom are also tested.

To test and apply the numerical techniques, a model called COMSIM (complex flow simulations) has been developed. The model has been tested and verified with the experimental results provided by Tsujimoto & Kitamura (1990).

METHODOLOGY

The Q3D numerical model, COMSIM, is constructed by coupling the SWM (shallow water module) with a finite difference based vertical unit. In the SWM, 2D shallow water equations are solved using the finite volume method with the Osher shock capturing scheme (Erduran *et al.* 2002). In the vertical unit the Navier–Stokes equations are

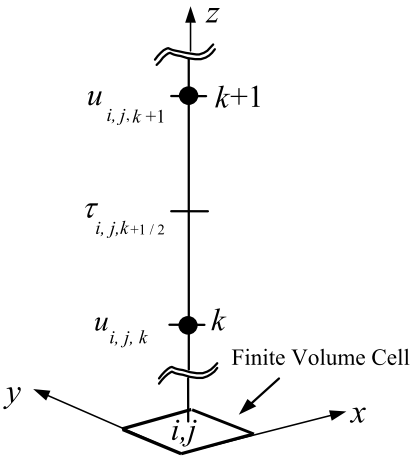

Figure 1 | Grid implementation.

solved in the vertical direction (in the z direction) using the finite difference method on vertical grids situated in the centres of the finite volume cells used in the SWM (Figure 1). In order to establish a Q3D solution, the water depth is obtained from the solution of the 2D shallow water equations and used in the solution of the Navier–Stokes equations with a hydrostatic pressure distribution providing vertical distribution of velocities and shear stresses.

Equations

The two-dimensional form of the shallow water equations can be written as:

$$\frac{\partial h}{\partial t}+\frac{\partial(hv_x)}{\partial x}+\frac{\partial(hv_y)}{\partial y}=0 \tag{1}$$

$$\frac{\partial(hv_x)}{\partial t}+\frac{\partial(hv_x^2+gh^2/2)}{\partial x}+\frac{\partial(hv_xv_y)}{\partial y}=gh(So_x-Sf_x)-\bar{F}_x \tag{2}$$

$$\frac{\partial(hv_y)}{\partial t}+\frac{\partial(hv_xv_y)}{\partial x}+\frac{\partial(hv_y^2+gh^2/2)}{\partial y}=gh(So_y-Sf_y)-\bar{F}_y \tag{3}$$

where h is the water depth, v_x, v_y represent the depth-averaged velocity components in the x and y directions respectively, g is the acceleration due to gravity, So_x and Sf_x are the bed slope and friction terms, respectively, in the x direction (similarly, So_y and Sf_y are in the y direction) and $\bar{F}_x$ and $\bar{F}_y$ are the averaged drag forces in the x and y directions, due to vegetation.

The reader may refer to Erduran *et al.* (2002) for the solution to Equations (1)–(3). The Navier–Stokes equations, including the drag forces, can be given as

$$\frac{\partial u_x}{\partial x}+\frac{\partial u_y}{\partial y}+\frac{\partial u_z}{\partial z}=0 \tag{4}$$

$$\frac{\partial u_x}{\partial t}-\frac{1}{\rho}\frac{\partial \tau_x}{\partial z}+F_x+u_x\frac{\partial u_x}{\partial x}+u_y\frac{\partial u_x}{\partial y}+u_z\frac{\partial u_x}{\partial z}+g\frac{\partial h}{\partial x}-gSo_x=0 \tag{5}$$

$$\frac{\partial u_y}{\partial t}-\frac{1}{\rho}\frac{\partial \tau_y}{\partial z}+F_y+u_x\frac{\partial u_y}{\partial x}+u_y\frac{\partial u_y}{\partial y}+u_z\frac{\partial u_y}{\partial z}+g\frac{\partial h}{\partial y}-gSo_y=0 \tag{6}$$

where u_x, u_y and u_z are velocity components in the x, y and z directions, respectively, ϱ is the density of water, τ_x and τ_y are vertical shear stresses in the x and y directions, respectively, and F_x and F_y are the drag forces per unit area due to vegetation in the x and y directions, respectively. The vertical shear stresses are represented in terms of vertical viscosity and the vertical gradient of horizontal velocities, as shown in Equation (7):

$$\frac{\tau_\lambda}{\rho}=\varepsilon_\lambda\frac{\partial u_\lambda}{\partial z},\ \lambda=x,\ y \tag{7}$$

where ε_x and ε_y are vertical eddy viscosities along the x and y directions respectively.

We also assume that the horizontal turbulent shear stresses are negligible as they are very small compared to the vertical turbulent shear stresses (Tan 1992). However, their effects can be important, especially for a partially vegetated flow domain; this needs to be further investigated. The momentum equation in the vertical direction is also omitted. Hence, a solution is Q3D.

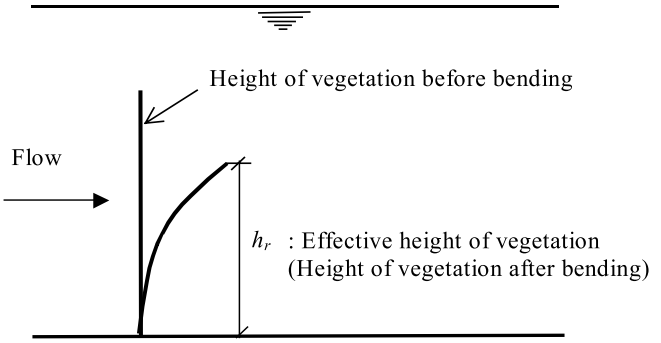

Figure 2 | Effective height of vegetation used in the computation of drag forces.

The drag forces, F_x and F_y, in the x and y directions due to vegetation are zero above the vegetation and inside the vegetative water zone they can be computed as

$$F_x = m\frac{h_r C_d u_x\sqrt{u_x^2+u_y^2}d}{2\Delta z} \qquad F_y = m\frac{h_r C_d u_y\sqrt{u_x^2+u_y^2}d}{2\Delta z} \tag{8}$$

where m is the density of vegetation (i.e. number of vegetations per unit area), C_d is a drag coefficient, d is the diameter of a vegetation and h_r is effective height of a vegetation (see Figure 2).

The vertical shear stresses (more specifically, the computation of the vertical eddy viscosity) are computed in two different ways, called method 1 and method 2 and explained below.

Method 1: a parabolic eddy viscosity approach with a correction term

For non-vegetated flow conditions, a parabolic eddy viscosity approach, given in Equation (9), had been previously used by Jin & Kranenburg (1993):

$$\varepsilon_\lambda = \kappa\left|(u^*_{b\lambda})\right| Z\left[1-\frac{Z}{h}\right], \lambda = x, y \tag{9}$$

where $\varkappa$ is the von Karman coefficient ($\varkappa = 0.41$), Z is the vertical elevation from the bottom and $u^*_{b\lambda}$ is the bed friction velocities.

Our experiences show that Equation (9) produces excessively large velocities over the tip of the submerged vegetation. Hence, a correction term based on our numerical experiments has been added. The resulting expression for the computation of the vertical viscosity is

$$\varepsilon_\lambda = \kappa\left|(u^*_{b\lambda})\right| Z\left[1-\frac{Z}{h}\right] + Z^* C_d^* u_\lambda \frac{|\Delta u_\lambda|}{|u^*_{b\lambda}|}, \lambda = x, y \tag{10}$$

Since Equation (10) is based on numerical experiments, it requires physical experimental justification.

The bed friction velocity can be computed by first applying the law of the wall rule (meaning that a logarithmic velocity distribution is assumed between the first grid point and the grid point above it), which can be given as

$$u_\lambda = \frac{u^o_\lambda}{\kappa}\ln\left[\frac{Z}{Z_0}\right], \lambda = x, y \tag{11}$$

where Z_0 is the equivalent roughness height which should be prescribed for every finite volume cell, and u^o_x and u^o_y are reference friction velocities related to the bottom shear stresses.

Jin & Kranenburg (1993) show that u^o_x and u^o_y can be computed by

$$(u_\lambda)_{k=1} = \frac{u^o_\lambda}{\kappa}\ln\left[\frac{Z_1}{Z_0}\right], \lambda = x, y \tag{12}$$

where Z_1 is the vertical elevation at grid point $k = 1$, and

$$(u^*_{b\lambda}) = Z\left[1-\frac{Z}{h}\right]\frac{u^o_\lambda}{Z_0}, \lambda = x, y \tag{13}$$

Now, u^o_x and u^o_y can be computed using Equation (12) in the x and y directions. Thus, u^*_{bx} and u^*_{by} are computed by using Equation (13). Once they are known, the vertical distribution of the eddy viscosity can be computed using Equation (10) and hence the vertical shear stresses can also be computed.

Method 2: Kutija and Hong's approach

For computation of the viscosity values for vegetated flow, Kutija & Hong (1996) combine the eddy viscosity and

mixing length theories. The border between the two layers (one using the eddy viscosity and another using the mixing length theory) is defined by a product of a parameter p_r (less than unity) and the effective vegetation height, h_r. The parameter p_r was introduced by Kutija & Hong (1996) as a better representation of flow behaviour near the tip of the vegetation by reducing the eddy viscosity layer. The vertical eddy viscosity inside the layer below the point $p_r h_r$ is computed using Equation (14), introduced by Tsujimoto & Kitamura (1990):

$$\varepsilon_\lambda = \alpha s_\lambda u_\lambda,\ \lambda = x,\ y \tag{14}$$

where α is an empirical coefficient and s_x and s_y are the distances between the vegetations in the x and y directions, respectively.

Above the point $p_r h_r$, the vertical eddy viscosity is computed using the mixing length theory (Jansen *et al.* 1979) expressed as

$$\varepsilon_\lambda = l_m^2 \left| \frac{\partial u_\lambda}{\partial z} \right| \tag{15}$$

where l_m is a mixing length which can be expressed as

$$l_m = \kappa Z \left(1 - \frac{Z}{h}\right)^{0.5}$$

Apart from the use of two different methods, two alternative boundary conditions for the bottom boundary are also applied in the solution of the Navier–Stokes equations. The first one is a non-slip boundary, where the velocities (u_x, u_y) at Z_0 above the bed vanish. The second boundary condition expresses the bottom shear stresses as functions of the average velocities and Manning's coefficient, n (Tan 1992). The former is applied for method 1 and the latter is used for method 2. The differences between these two methods are summarized and given in Table 1.

Table 1 | Differences in available solutions in COMSIM for Q3D flow simulation

Solution	Shear stress computations	Bottom boundary
Method 1	Parabolic eddy viscosity and additional formula	Non-slip
Method 2	Empirical formula and mixing length theory	Friction formula

Bending

Kutija & Hong (1996) introduce a solution for flow through flexible vegetation. The solution is based on the relationship between load acting on the vegetation, resulting from the flow velocity, and the deflection of the vegetation due to that load. This solution is explained here.

The load on the vegetation is caused by the flow and the magnitude of the load depends on the velocity. The load is represented by discrete portions of constant load distributed over the height of the vegetation and can be computed for the x direction as

$$(q_{lx}) = \frac{C_d d (u_x) \sqrt{(u_x)^2 + (u_y)^2}}{2} \tag{16}$$

For the y direction, the subscript x is replaced by y and y is replaced by x. Note that the load is computed at every (i,j,k) point in the vegetated layer.

The deflection at any point along the vegetation height is computed using cantilever beam theory (Timoshenko 1955). According to this theory, together with a superposition method, the deflection of a beam (in this case the vegetation) at any point, caused by individual loads acting separately, is equal to the sum of the deflections caused by these loads.

Kutija & Hong (1996) state that, depending on the position of a point relative to the position of the load, the deflection of the point on the cantilever beam is expressed in different ways. For instance, Equation (17) is applied when the point is inside the border of the fixed end of the beam and the beginning of the load, whereas Equation (18) is applied when the point is between the loads and the free end of the beam (see Figure 3). As Kutija & Hong (1996) explain, the deflection of a point inside the load is not needed due to the discrete nature of the solution.

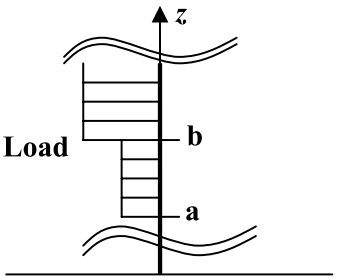

Figure 3 | The points on the vegetation, where the deflection is computed.

For $z \le a$:

$$\delta'_\lambda = \int_a^b \frac{(q_{l\lambda})z^2}{6EI}(3c - z)\mathrm{d}c,\ \lambda = x, y \tag{17}$$

For $z \ge b$:

$$\delta''_\lambda = \int_a^b \frac{(q_{l\lambda})c^2}{6EI}(3z - c)\mathrm{d}c,\ \lambda = x, y \tag{18}$$

where EI is the stiffness of the beam, and δ'_λ and δ''_λ are deflections at the points $z \le a$ and $z \ge b$, respectively.

It should be noted that Equations (17) and (18) are derived based on an assumption that the deflection is small. The deflection is calculated for every point halfway between two discretisation points (k^{th} points). The total deflection at a point m is given by

$$(\delta_m^T) = \sum_{k=1}^{m} \delta'_{m,k} + \sum_{k=m+1}^{k_1} \delta''_{m,k} \tag{19}$$

where δ_m^T denotes the total deflection at point m.

The net deflection of each element, δ_k^N, is expressed as

$$\delta_k^N = \delta_{k+\frac{1}{2}}^T - \delta_{k-\frac{1}{2}}^T \tag{20}$$

After the deflection, the vegetation length inside each k^{th} element is computed as

$$l_k = \sqrt{(\delta_k^N)^2 + (\Delta z_1)^2} \tag{21}$$

where l_k is the vegetation length for the k^{th} element and Δz_1 is the space step within the vegetative water course.

The height of the vegetation is then distributed over the lengths of the elements to calculate the effective vegetation height, h_r. The load causes a reduction in the effective vegetation height due to the bending but when the effective vegetation height is reduced the load acting on the vegetation is also reduced. The reduced load causes less bending than the previous load does. In order to deal with these interrelated processes, an iterative procedure is applied. In each step, the new load and the new effective height are computed. Iteration ceases when there is not much change (i.e. 0.01 m) between the effective vegetation heights computed at two consecutive steps.

Solution to the Navier–Stokes equations

Acceleration terms, drag forces and computation of the shear stresses are discretised using an implicit scheme. The remaining terms are treated explicitly to decrease the computational effort. In the discretisation of advective terms, ordinary upwind discretisation is used (Tan 1992). The horizontal gradients of water depth are approximated using a forward difference approximation. Following Jin & Kranenburg (1993), the advective terms are also approximated in such a way that the occurrence of non-orthogonal grids as a result of the water level variation in the vertical directions is taken into account. Although the use of non-orthogonal grids increases the computational effort, it was deemed to be the best option because it allows the model to be set up with the same number of grid points above each finite volume cell.

The unknown velocities are computed at all the discretisation points but the vertical shear stresses are computed halfway between each set of two grid points (see Figure 1).

In method 1, the vertical grid spacing (Δz_2) used is constant and an equal number of grid points is used for all verticals. However, as shown in Figure 4, the first grid point, $k = 0$, is placed Z_0 above the bottom and the final grid point, $k = kk$, is placed half a grid spacing below the free surface.

In method 2, due to the computation of the vertical turbulent shear stresses in two different ways along the vertical direction, the grid points are placed in such a way

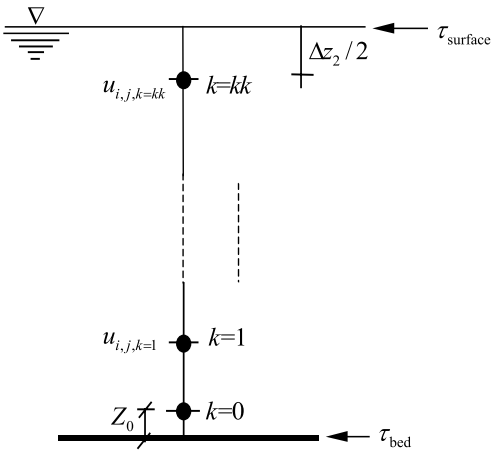

Figure 4 | Vertical grid used in method 1.

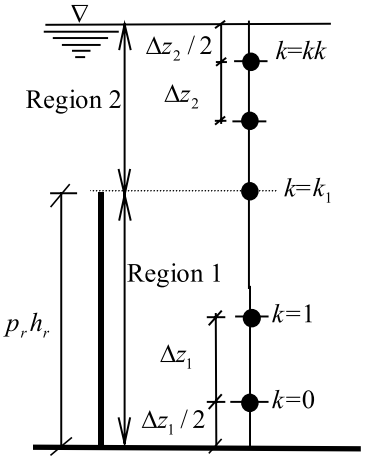

Figure 5 | Grid spacing used in method 2.

that a discretisation point is maintained at the boundary between the regions using eddy viscosity and mixing length theory. Consequently, for each region, the space interval size is separately computed (see Figure 5).

For region 1 (below the point $p_r h_r$):

$$\Delta z_1 = \frac{p_r h_r}{k_1 + 0.5} \tag{22}$$

where subscript 1 denotes the region number and k_1 refers to the number of grid points in region 1.

For region 2 (above the point $p_r h_r$):

$$\Delta z_2 = \frac{h - p_r h_r}{k_2 + 0.5} \tag{23}$$

where subscript 2 denotes the region number and k_2 is the number of grid points in region 2.

The final discretised form of the x momentum Equation (5), for the case u_x, u_y and u_z all less than zero (different cases occur due to upwind discretisation, which depends on the sign of flow direction), can be given for method 1 as shown in Equation (24):

$$A_{(i,j,k)}(u_x)^{n+1}_{(i,j,k-1)} + B_{(i,j,k)}(u_x)^{n+1}_{(i,j,k)} + C_{(i,j,k)}(u_x)^{n+1}_{(i,j,k+1)} = D_{(i,j,k)} \tag{24}$$

where

$$A_{(i,j,k)} = -r_2$$

$$B_{(i,j,k)} = \left[1 + r_1 + r_2 + \frac{\Delta t m C_d}{2\Delta z} d_{(i,j,k)} (h_r)^n_{(i,j,k)} \sqrt{[(u_x)^n_{(i,j,k)}]^2 + [(u_y)^n_{(i,j,k)}]^2} \right]$$

$$C_{(i,j,k)} = -r_1$$

$$D_{(i,j,k)} = (u_x)^n_{(i,j,k)}(1 - r_1 - r_2 + r_3 + r_4) + (u_x)^n_{(i,j,k+1)}(r_1 - r_3) + (u_x)^n_{(i,j,k-1)}(r_2 - r_4) -$$

$$\Delta t (u_x)^n_{(i,j,k)} \left[\frac{(u_x)^n_{(i+1,j,k)} - (u_x)^n_{(i,j,k)}}{\Delta x} - \frac{(u_x)^n_{(i,j,k+1)} - (u_x)^n_{(i,j,k)}}{\Delta z} \left(\frac{Z_{(i+1,j,k)} - Z_{(i,j,k)}}{\Delta x} \right) \right] -$$

$$\Delta t (u_y)^n_{(i,j,k)} \left[\frac{(u_x)^n_{(i,j+1,k)} - (u_x)^n_{(i,j,k)}}{\Delta y} - \frac{(u_x)^n_{(i,j,k+1)} - (u_x)^n_{(i,j,k)}}{\Delta z} \left(\frac{Z_{(i,j+1,k)} - Z_{(i,j,k)}}{\Delta y} \right) \right] -$$

$$\Delta t(u_z)^n_{(i,j,k)}\left[\frac{(u_x)^n_{(i,j,k+1)}-(u_x)^n_{(i,j,k)}}{\Delta z}\right]-$$

$$\Delta tg\left[\frac{(h)^{n+1}_{(i+1,j)}-(h)^{n+1}_{(i,j)}}{\Delta x}\right]+\Delta tgS_{ox}$$

$$r_1=\frac{\theta\Delta t}{(\Delta z)^2}(\varepsilon_x)_{(i,j,k+½)},\ r_3=\frac{\Delta t}{(\Delta z)^2}(\varepsilon_x)_{(i,j,k+½)},\ r_2=$$

$$\frac{\theta\Delta t}{(\Delta z)^2}(\varepsilon_x)_{(i,j,k-½)},$$

$$r_4=\frac{\Delta t}{(\Delta z)^2}(\varepsilon_x)_{(i,j,k-½)}$$

θ is a weighting coefficient, taken to be 0.51, and

$$\varepsilon_{x(i,j,k+½)}\approx\frac{\varepsilon_{x(i,j,k+1)}+\varepsilon_{x(i,j,k)}}{2},\ \varepsilon_{x(i,j,k-½)}\approx\frac{\varepsilon_{x(i,j,k)}+\varepsilon_{x(i,j,k-1)}}{2}$$

The coefficients $A_{(i,j,k)}$, $B_{(i,j,k)}$, $C_{(i,j,k)}$ and $D_{(i,j,k)}$ defined above have all values known at the time level n and the water depth, h^{n+1}, is taken from the 2D depth-averaged model so it is also known. Equation (24) is written for each discretisation point in the vertical direction. This provides a system of linear algebraic equations. The number of equations is equal to the number of grid points in the vertical direction. The unknown horizontal velocities can be computed using a double-sweep algorithm (Abbott & Minns 1998) since the matrix of the system is tri-diagonal. The discretised equations for method 2 are in exactly the same form as that given by Equation (6). However, for method 2, the coefficients $A_{(i,j,k)}$, $B_{(i,j,k)}$, $C_{(i,j,k)}$ and $D_{(i,j,k)}$ are redefined and computation of the coefficients is achieved by considering seven different cases resulting from the estimation of the shear stresses in different ways and applying boundary conditions. For details consult Kutija & Hong (1996) and Erduran (2001).

The solution requires two boundary conditions, one at the bed and another at the free surface. For both methods we use a slip boundary condition (no shear stress, i.e. $\tau_{x(i,j,kk+1/2)}=0$) at the free surface. At the bottom, a non-slip boundary condition is used for method 1. This means that the horizontal velocity, $(u_x)_{i,j,0)}$, at the vertical point $k=0$, is taken to be zero. Hence, the coefficients, $A_{(i,j,0)}$ and $B_{(i,j,0)}$, are set to zero. Apart from the above condition, the law of the wall rule is used. Therefore, a logarithmic velocity distribution is assumed between the non-slip grid point ($k=0$) and the grid point above ($k=1$). In method 2, bottom friction is computed using a resistance law (Tan 1992). For instance, in the x direction, it can be given as

$$\frac{\tau_{bx}}{\rho}=\frac{n^2(\bar{u}_x)\sqrt{(\bar{u}_x)^2+(\bar{u}_y)^2}}{h^{4/3}} \tag{25}$$

where $\bar{u}_x$ and $\bar{u}_y$ are the depth-averaged velocities in the x and y directions respectively and n is Manning's coefficient.

The average velocities can be computed as

$$\bar{u}_\lambda=\frac{\sum_{k=0}^{kk}(u_\lambda)_{(i,j,k)}}{kk+1},\ \lambda=x,\ y \tag{26}$$

The solution in the y direction can be achieved in the same way. Note that these averaged velocities should be equal to the depth-averaged velocities obtained from the SWM. However, the solution in the SWM is based on the finite volume method whereas the solution used in the vertical unit is based on the finite difference method. Moreover, different approximations are used in the SWM and the vertical unit. Thus, the depth- averaged velocities obtained from solution of the shallow water equations are slightly different than the depth-averaged velocities computed using Equation (26). These initially small differences can result in larger differences (cumulative error) as the computation proceeds. Therefore, the correction procedure for the velocities obtained from the vertical unit has to be applied (Jin & Kranenburg 1993).

The vertical velocity at each grid point can be computed from the continuity equation (4). Note that corrections of the discretised terms in Equation (4), due to the occurrence of non-orthogonal grids, should also be made.

Coupling

A Q3D module is constructed by coupling the shallow water module (SWM) with the vertical unit. The SWM and

Table 2 | Data used in model simulations

Time step, Δt	0.1 sec	Drag coefficient, C_d	1.1
Bottom slope	0.0001	Numerical parameter, p_r	0.75
Manning's n	0.01	Numerical parameter, α	0.01
Water depth	3 m	Vegetation diameter at the bottom, d_b	0.002 m
Vegetation length, h_r	1.25 m	Vegetation diameter at the top, d_t	0.002 m
Vegetation density, m, per m^2	100	Range of stiffness values, (EI), tested	0.006–3 N m^2
Roughness height, Z_0	0.01 m		
Channel length	60 m	Channel width	1 m
Number of cells	60	Cell size	1 m × 1 m
Horizontal boundary conditions			
Upstream: Water depth	3 m	Downstream: Open	
Remaining boundaries on left and right sides of the channel are a closed boundary			
Simulations are completed when the steady state condition is achieved, i.e. 6000 sec			

the vertical unit are coupled by passing data between them. These are the water depth, the bottom shear stresses (if method 1 is used) and the averaged drag forces. The water depth is computed in the SWM and used as input into the vertical unit. Receiving the water depth from the SWM is the main feature of the Q3D solution. The bottom shear stresses and the averaged drag forces are evaluated in the vertical unit and are fed back into the SWM using the splitting technique (Toro 1997; Erduran *et al.* 2002). The averaged drag forces can be computed by

$$\bar{F}_\lambda = \frac{\sum_{k=0}^{kk} (F_\lambda)_{(i,j,k)}}{kk+1} h\,,\ \lambda = x,\ y \tag{27}$$

The bottom shear stresses are computed as

$$\frac{\tau_{b\lambda}}{\rho} = |u^*_{b\lambda}| u^*_{b\lambda}\,,\ \lambda = x,\ y \tag{28}$$

Note that, when method 1 is selected, Equation (28) is used instead of Sf_λ ($\lambda = x,y$) in Equations (2) and (3). For method 2, the bottom friction terms (Sf_λ) are computed using Equation (25) but $\bar{u}_x$ and $\bar{y}_y$ are replaced by v_x and v_y.

MODEL APPLICATIONS TO FLEXIBLE VEGETATION

Unfortunately, no suitable experimental data were available to test COMSIM for cases with flexible vegetation. Therefore, we have applied the model to artificial data used by Kutija & Hong (1996) in order to illustrate that the model can deal with flexible vegetation. Overall data are illustrated in Table 2.

Figure 6 shows that the deflection at the tip of the vegetation is 0.20 m when the stiffness value is taken to be 0.05 N m^2, which corresponds to a grass–legume mixture in fall and spring in nature (Kouwen *et al.* 1981) and the vegetation height is reduced to 0.018 m. The use of stiffness values higher than 0.05 N m^2 results in little or no

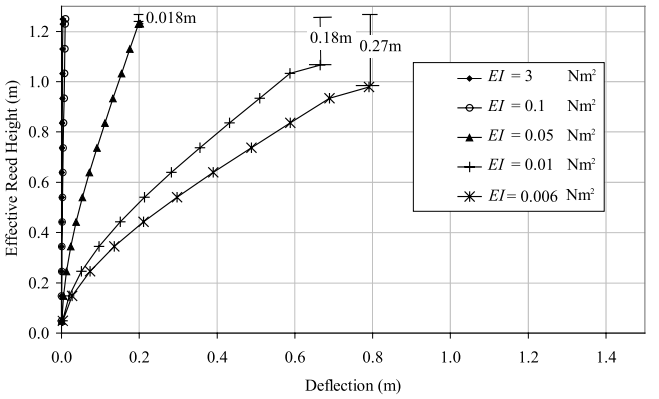

Figure 6 | Deflection of vegetation.

Table 3 | Data used by Tsujimoto & Kitamura (1990)

Run*	Water depth (cm)	Bottom slope	Condition of cylinders
A11	9.50	0.001	Submerged
A31	9.36	0.003	Submerged
A14	3.00	0.001	Non-submerged
A71	8.95	0.007	Submerged

*Named by Tsujimoto & Kitamura (1990).

deflection. However, lower values of stiffness cause considerable deflections. For example, stiffness values of 0.01 and 0.006 N m^2 result in total deflections of 0.67 and 0.79 m, respectively. These deflections are extensive in relation to the 1.25 m vegetation height and that might be in breach of the assumption of small deflection used in Equations (17) and (18). Due to this limitation, the model's application to an experimental example involving highly flexible vegetation is still under investigation.

MODEL CALIBRATION AND VERIFICATION

The calibration and verification of our model are accomplished through the experimental data given by Tsujimoto & Kitamura (1990) for rigid vegetation only. Tsujimoto & Kitamura (1990) conducted an experiment in a 12 m long, 0.4 m wide flume with an adjustable bottom slope. Cylinders made of bamboo represented the vegetation. The diameter of each cylinder is 0.15 cm and the height 4.59 cm. They set up the cylinders 2 cm apart in both the x and y directions. Therefore, the distance between each cylinder is 2 cm. The other data used in their experiments are presented in Table 3.

In the application of the model, the computational domain is divided into 12×1 horizontal cells. Each cell has a size of $0.4\ m \times 1\ m$. The number of vertical grid points used is 20 for submerged cases and 7 for a non-submerged case. It is noted that, in order to capture more accurately the variations in the vertical velocity profile, the vertical grid size (Δz) should be small. The same applies to computation of deflection of submerged-flexible vegetation. The boundary conditions are set up as follows. The upstream boundary is chosen to be a water depth (for each run the water depth at the upstream boundary is equal to the water depth given in Table 3). The downstream boundary is given as an open boundary for all runs. The time step of 0.2 s is used for all simulations. The simulations are completed when the steady state condition is achieved in a channel.

The calibration of COMSIM was achieved by comparing the model results with the results given by Tsujimoto & Kitamura (1990) for run A11. Once agreement between the model and the experimental results was obtained, the calibration was completed. In the use of method 1, the roughness height (Z_0) and the drag coefficient (C_d) were calibrated, as they are the only parameters that require calibration. For method 2, the following parameters were calibrated: the coefficients p_r, α, C_d and Manning's n. The calibrated parameters are given in Table 4. Individual effects of these parameters on the flow behaviour and their significance can be found in Kutija & Hong (1996) and Erduran (2001). Briefly, in the above references it is shown that the most significant parameters are the properties of the vegetation such as the vegetation height, diameter, stiffness and density. While the coefficient p_r is also found to play a significant role, the coefficient α is found to be insignificant.

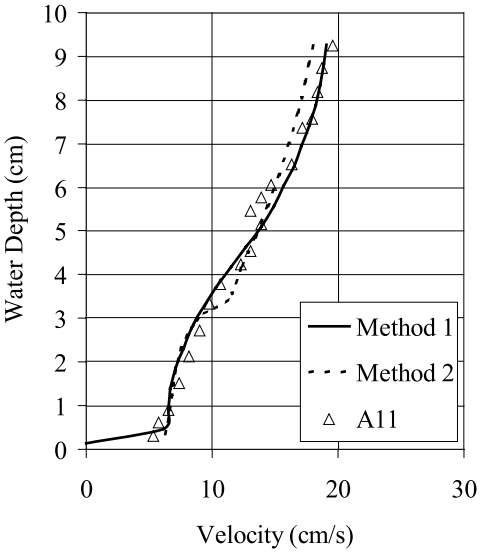

Figure 7 | Vertical distribution of the horizontal velocities obtained from COMSIM and A11.

Table 4 | Calibrated parameters

Method	z_0 (m)	p_r	α	c_d	n
1	0.0009	—	—	1.1	—
2	—	0.75	0.005	1.1	0.024

The results of COMSIM, using methods 1 and 2 versus the result of A11 used for calibration, are plotted in Figure 7.

The calibrated parameters given in Table 4 are used for the other runs, A31, A71 and A14, for verification of the model. The results are illustrated in Figure 8(a), (b) and (c), respectively.

It can be said that, apart from run A31, in which the model produced slightly larger velocities than those obtained from the experiment, overall results are quite satisfactory. In Figures 7 and 8(a), (b) one can observe that the results of method 2 show a velocity bulge around the tip of the effective vegetation height. This is expected due to the different way of shear stress computation below and above that point used in that method. The results for run A14 show that, in the non-submerged vegetation case, the velocity profile is almost a straight line (constant) over the

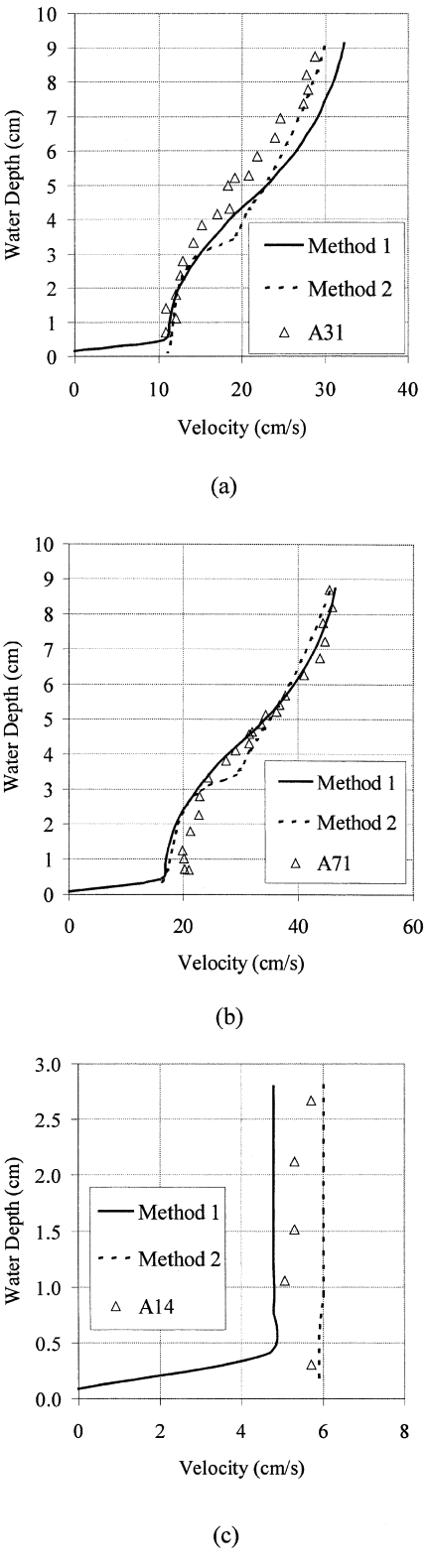

Figure 8 | Vertical distribution of the horizontal velocities obtained from COMSIM and A31 (a), A71 (b) and A14 (c).

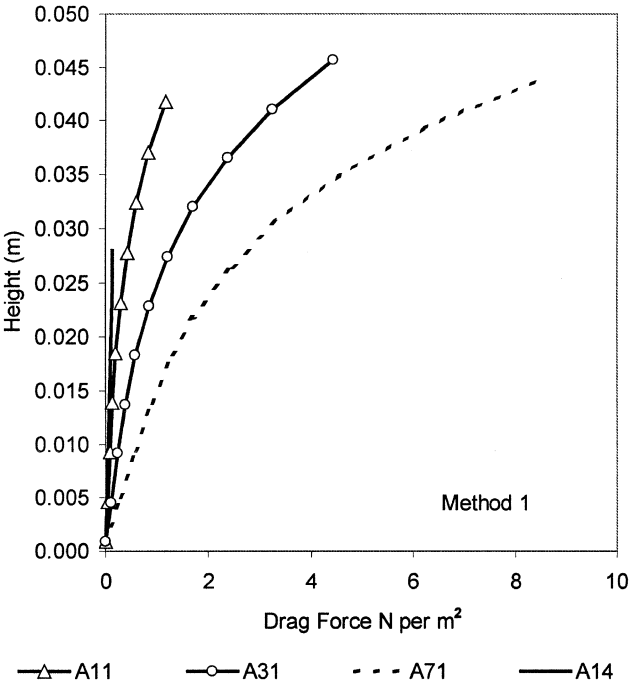

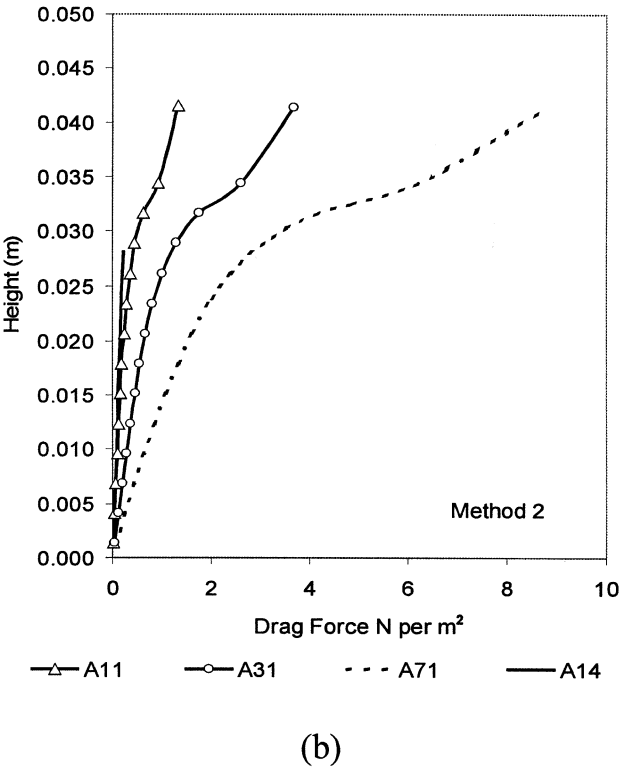

Figure 9 | Drag forces obtained using (a) method 1 and (b) method 2.

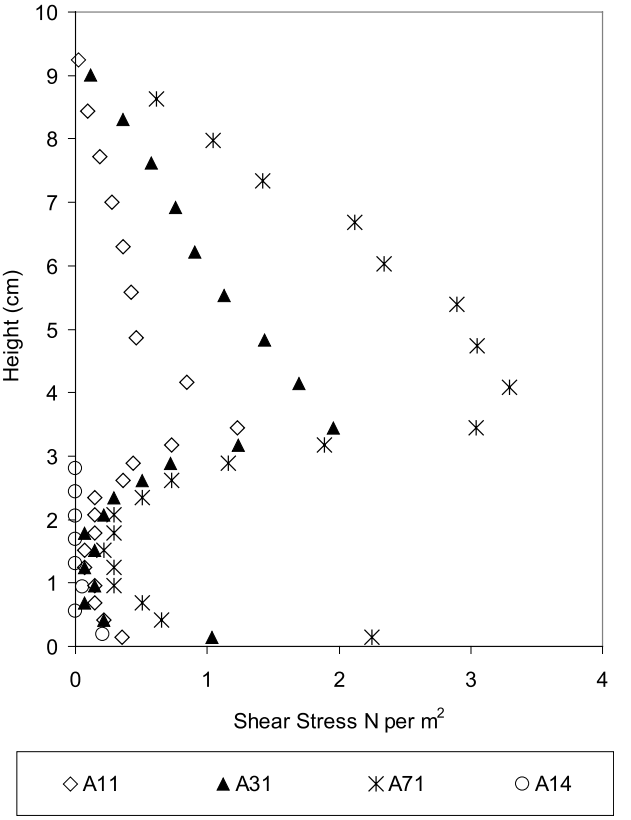

Figure 10 | Shear stress distribution obtained from method 2.

water depth. From this point, it may be concluded that, in such cases, use of just a two-dimensional horizontal numerical model would give satisfactory results. In submerged vegetation conditions, it is essential to use a model capable of giving a vertical velocity distribution.

In Figures 7 and 8(a, b), representing submerged vegetation cases, three regions can be distinguished. The first region is near bed, where the shape of the profile is dominantly affected by the bed friction. The second region, in which the velocity profile has a more or less convex shape, is a vegetated region. In this region drag forces play an important role. The third region, in which the profile is concave, is the surface flow region. The more obvious change in the velocity profile occurs at the boundary between the surface flow and vegetated flow layers (the shape of the velocity profile changes from convex to concave). This occurs due to the transition from slower flow, caused by vegetation, to the faster flow in the surface flow layer.

In method 1, a non-slip boundary condition is used at the bottom and it is assumed that the velocity profile between the first two grid points is logarithmic. These two assumptions are widely recognized (Jansen *et al.* 1979). Also, the bottom shear stress should be related to the velocity near the bottom (Tan 1992) and not to the averaged velocity, as it is in method 2.

As expected, the velocities increase when the bottom slope increases. Similarly, drag forces increase (Figure 9).

The drag forces obtained from both methods are similar. The trend of the drag force profile obtained from method 2 shows a sudden change at a point (height $= p_r h_r$) as expected. The shear stress profiles obtained for submerged and non-submerged vegetation cases are similar to the turbulence intensity profiles reported by Tsujimoto & Kitamura (1990) and are given in Figure 10.

CONCLUSIONS

From this study, the following conclusions can be drawn:

1. A Q3D model with two alternative turbulence closure approaches was introduced for flow through flexible and rigid, submerged and non-submerged vegetation.
2. The model was calibrated and verified using the experimental data provided by Tsujimoto & Kitamura (1990) for the rigid vegetation case. The results are found to be satisfactory.
3. Although the model could not be verified with the flexible vegetation experimental data due to incompatibilities in parameters and assumptions we demonstrated how it can deal with flexible vegetation.
4. It is hoped that the Q3D solution algorithm introduced here will be useful for studies involving ecology, hydrology and hydraulics.

FUTURE WORK

Turbulence closure is achieved by using rather simple approaches. Although the results are quite satisfactory and the algorithm for flexible vegetation has already brought enough complexity, it may be still worth trying a more up-to-date turbulence closure method (i.e. the $k-\varepsilon$ model) together with a fully 3D solution that deals with non-hydrostatic pressure distribution. This would be particularly useful for simulation of flow at the tip of submerged vegetation because of the highly turbulent characteristics of the flow and the occurrence of the non-hydrostatic pressure distribution at this point.

ACKNOWLEDGEMENT

The first author would like to thank the Turkish Republic Ministry of National Education for their financial support.

NOTATION

h: water depth
v_x and v_y: depth-averaged velocity components in the x and y directions, respectively
g: acceleration due to gravity
So_x and So_y: bed slope in the x and y direction, respectively
Sf_x and Sf_y: friction terms in the x and y direction, respectively
u_x, u_y and u_z: velocity components in the x, y and z directions, respectively
ϱ: density of water
τ_x and τ_y: vertical shear stresses in the x and y directions, respectively
F_x and F_y: drag forces in the x and y directions, respectively
ε_x and ε_y: eddy viscosities along the x and y directions, respectively
m: density of vegetation
C_d: drag coefficient
d: diameter of a reed
h_r: effective reed height
$\varkappa$: von Karman coefficient, $\varkappa = 0.41$
Z: vertical elevation from the bottom
u^*_{bx} and u^*_{by}: bed friction velocities in the x and y directions, respectively
Z_0: equivalent roughness height

u_x^o and u_y^o: reference friction velocity related to the bottom shear stress

τ_{bx} and τ_{by}: bottom shear stresses in the x and y directions, respectively

l_m: mixing length

α: empirical coefficient

s_x and s_y: distances between the reeds in the x and y directions, respectively

p_r: coefficient, less than unity

q_{lx} and q_{ly}: Partial loads in the x and y directions, respectively

EI: stiffness of the beam (reed)

δ' and δ'': deflections

δ_m^T: total deflection

δ_k^N: net deflection

l_k: reed length for kth element

Δz: space step

$\overline{u}_x$ and $\overline{u}_y$: computed depth averaged velocities in the x and y directions respectively

n: Manning's roughness coefficient

$\bar{F}_x$ and $\bar{F}_y$: average drag forces in the x and y directions, respectively.

REFERENCES

Abbott, M. B. & Minns, A. W. 1998 *Computational Hydraulics*. 2nd Edition. Ashgate, Aldershot, UK.

Chow, V. T. 1973 *Open-Channel Hydraulics*. International Edition. McGraw-Hill, Singapore.

Darby, S. E. 1999 Effect of riparian vegetation on flow resistance and flood potential. *J. Hydraul. Eng.* **125**, 443–454.

Erduran, K. S. 2001 *An Integrated Model for Complex Flow Simulations: COMSIM.* PhD thesis, unpublished, University of Newcastle upon Tyne, UK.

Erduran, K. S., Kutija, V. & Hewett, C. J. M. 2002 Performance of finite volume solutions to the shallow water equations with shock-capturing schemes. *Int. J. Num. Methods Fluids* **40**, 1237–1273.

Fischenich, C. 2000 Resistance due to vegetation. *EMRRP Technical Notes*, ERDC TN-EMRRP-SR-07, US Army Engineer Research and Development Center, Vicksburg, MS.

Fischer-Antze, T., Stoesser, T., Bates, P. & Olsen, N. R. B. 2001 3D numerical modelling of open-channel flow with submerged vegetation. *J. Hydraul. Res*. **39**, 303–310.

Jansen, P., Bendegom, L., Berg, J., Vries, M. & Zanen, A. 1979 *Principles of River Engineering*. Pitman, London.

Jin, X. & Kranenburg, C. 1993 Quasi-3D numerical modelling of shallow-water circulation. *J. Hydraul. Eng*. **119**, 458–472.

Kouwen, N. & Li, R.-M. 1980 Biomechanics of vegetative channel linings. *J. Hydraul. Div. ASCE* **106**, 1085–1102.

Kouwen, N., Li, L.-M. & Simons, D. B. 1981 Flow resistance in vegetated waterways. *Am. Soc. Agric. Engrs*. **24**, 684–690.

Kouwen, N. 1992 Modern approach to design of grassed channels. *J. Irrigation Drainage Engng*. **118,** 733–743.

Kutija, V. & Hong, H. T. M. 1996 A numerical model for assessing the additional resistance to flow introduced by flexible vegetation. *J. Hydraul. Res*. **34**, 99–114.

Li, R.-M. & Shen, H. W. 1973 Effect of tall-vegetation on flow and sediment. *J. Hydraul. Div. ASCE* **99**, 793–814.

Maghadam, M. F. & Kouwen, N. 1997 Nonrigid, nonsubmerged, vegetative roughness on floodplains. *J. Hydraul. Eng*. **123**, 51–57.

Petryk, S. & Bosmajian III, G. 1975 Analysis of flow through vegetation. *J. Hydraul. Div. ASCE* **101**, 871–884.

Saowapon, C. & Kouwen, N. 1989 A physically based model for determining flow resistance and velocity profiles in vegetated channels. In*: Proc. Int. Conf. on Flow and Catchment Runoff* May 22–26 (ed. Yen, B.C.), University of Virginia, Charlottesville, VA, USA, 559–568.

Shimizu, Y. & Tsujimoto, T. 1997 Suspended sediment concentration affected by organized motion near vegetation zone. In: *27th IAHR Congress on Environmental and Coastal Hydraulics: Protecting the Aquatic Habitat,* (ed. Wang, S.S.-Y.), ASCE, San Francisco, CA, vol. 2, pp 1384–1389.

Simoes, F. J. & Wang, S. S.-Y. 1997 Three-dimensional modelling of compound channels with vegetated flood plains. In: *27th IAHR Congress on Environmental and Coastal Hydraulics: Protecting the Aquatic Habitat,* (ed. Wang, S.S.-Y.). ASCE, San Francisco, CA, vol. 2, pp 809–814.

Tan, W. 1992 *Shallow Water Hydrodynamics*. Elsevier, Amsterdam.

Temple, D. M. 1986 Velocity distribution coefficients for grass-lined channels. *J. Hydraul. Eng.* **122**, 193–205.

Timoshenko, S. 1955 *Strength of Materials; Part 1: Elementary Theory and Problems*. Van Nostrand, New York.

Toro, E. F. 1997 *Riemann solvers and numerical methods for fluid dynamics*. Springer-Verlag, First Edition, Berlin.

Tsujimoto, T. & Kitamura, T. 1990 Velocity profile of flow in vegetated-bed channels. *KHL Progressive Report*, Hydraulic Laboratory, Kanazama University, Japan.

Wu, F.-C., Shen, H. W. & Chou, Y.-J. 1999 Variation of roughness coefficients for unsubmerged and submerged vegetation. *J. Hydraul. Eng*. **125,** 934–942.

Wu, Y., Falconer, R. A. & Struve, J. 2001 Mathematical modelling of tidal currents in mangrove forests. *Environ. Modell. Software*. **16**, 19–29.